DIFFERENTIAL CROSS SECTIONS IN ETA PHOTOPRODUCTION FROM 0.8 TO 1.45 GeV*

E. D. Bloom,† C. A. Heusch, C. Y. Prescott, and L. S. Rochester
California Institute of Technology, Pasadena, California
(Received 8 July 1968)

The cross section for the process $\gamma p \to p\eta$ was studied from 0.8- to 1.45-GeV incident photon energy at center-of-mass angles from 50 to 90°. The data cover a range of energies well beyond previous measurements. The results will aid in the study of $I=\frac{1}{2}$ nucleon isobars.

In this experiment we measured the differential cross section of the process

$$\gamma p \to p\eta(\eta \to 2\gamma) \quad (1)$$

by detecting all three particles in the final state, at incoming photon energies from 0.8 to 1.45 GeV, and at η center-of-mass angles between 40 and 100°.

The photoproduction of eta mesons derives its interest from two features; first, it can proceed through the $I=\frac{1}{2}$ channel only, so that it provides an unambiguous probe for nucleon isobars of isospin $\frac{1}{2}$; second, the position of η meson as the isosinglet in the 0^--meson SU(3) octet makes a comparison with the production of the $I=1, I_3=0$ π^0 fruitful. Since the γp vertex conserves U spin, SU(3) symmetry predicts definite coupling ratios for various exchanges and intermediate states. These are features which cannot be directly extracted from π production, or from processes of the type $\pi p \to \pi N$ and $\pi p \to \eta n$.

Existing data on η production in γp and πp collisions show two distinctive details: a sharp rise above threshold and a rapid decrease of the cross section occurring after a plateau of ~150-MeV width.[1] The onset and slope of the decrease appear to be different in the πN- and γN-initiated reactions.[2] There is fair evidence that in the region of the cross-section maximum, the angular distribution of η production is consistent with isotropy.[3] In addition, a flat cross-section region above the strong decrease spans the energy region of the nucleon isobar N_{15}***(1688).[4]

Several authors have made an attempt to account for this structure of the production cross section in terms of the nucleon isobars known from πN scattering and π photoproduction.[5] The steep rise above threshold and the apparent isotropy at the maximum of the cross section are ascribed to the formation and decay of the $N^*(S_{11}, 1570)$ which was observed, with high inelasticity, in πN scattering.[6] However, the steep decrease of the cross section, as exhibited by the existing data, is hard to explain even with the addition of other terms. There may be an admixture of a P_{11} state or of the $D_{13}(1512)$, although the latter is expected to be suppressed because of the angular momentum barrier. In addition, a specific search for the decay of the $F_{15}(1688)$[4] yielded an upper limit which allowed the assignment of this isobar to an SU(3) octet with $J^P=\frac{5}{2}^+$.[7] This SU(3) assignment, together with a ratio for symmetric to antisymmetric octet-octet coupling of $\alpha/(1-\alpha) \approx \frac{3}{2}$, accounts for the suppression of this intermediate state for the ηN final state.

In the present experiment we sought to (1) reduce the errors and fluctuations on the high-energy end of the ηN threshold enhancement, (2) obtain a limited angular distribution around the F_{15} (1668) energy region in order to check for F- or D-wave effects, and (3) extend the cross-section measurements to as high an energy as the California Institute of Technology 1.5-GeV electron synchrotron would permit.

The detection system for the final-state proton consisted of a spark-chamber telescope for proton detection (two thin-foil chambers for track delineation, defining the production angles to ~0.3° and a modular range chamber to stop the protons and determine their kinetic energy with a typical resolution of about 4 MeV) and a sequence of scintillator counters with pulse-height discrimination for triggering. The etas were detected through their decay mode into two photons, if it occurred symmetrically in a plane roughly perpendicular to the production plane. The photons passed through veto counters, a lead converter two radiation lengths thick, crossed scintillator hodoscopes to record the shower locations, and a lead-Lucite Čerenkov shower counter.[8] In this manner, the eta production and decay angles were determined to ~±0.5°, and a rough measurement of the individual shower energies was obtained for consistency purposes.

As indicated below, this procedure overdetermines the kinematics, and allows for an efficient suppression of the backgrounds which plague eta-photoproduction measurements. All kinematical

information was contained in one photographic frame per event, with a 90° stereoscopic view of the proton tracks, and digital information on the location and energy of both photon showers. The detection efficiency of the system was determined by means of a Monte Carlo calculation.[9]

Out of a total of 46000 frames, we analyzed 34000 and obtained about 6000 eta events. For each event, we calculated the kinematical parameters in two independent ways. First, we assumed that the objects triggering the two-photon hodoscopes were the decay products of one particle that decayed into two photons, so that the proton trajectory and the production angle θ allowed for the determination of that object's mass m and its energy E. Second, we calculated the "eta" energy E' from the angles of the two-photon directions with the production plane, and an assumed mass of 549 MeV. The difference between these two eta energy values $\Delta E = E - E'$ is plotted versus the apparent η mass m in Fig. 1. We expect events which satisfy eta production kinematics to fall in the vicinity of the point $m = 550$ MeV and $\Delta E = 0$. Events not satisfying eta kinematics come largely from processes such as $\gamma p \to p\pi^\circ\pi^\circ$, and $\gamma p \to p\eta(\eta \to 3\pi^\circ)$, with two photons in the final state simulating the two-photon decay of the eta. Figure 1 is a typical dot plot, containing a sample of events which were analyzed in one setting, before any kinematical constraints were applied. We note that there is an accumulation of events at the expected location. The resolution in both m and ΔE can be unequivocally calculated from known quantities (such as trajectory resolution, accuracy of range information, etc.), so that we can establish "allowed" eta bands for both parameters. The events falling outside the doubly allowed region in the center then provide a ready sample of background events, and make a subtraction under the peak straightforward.

In Fig. 2, we show the subtraction procedure for one kinematical setting; Fig. 2(a) shows the events from the ΔE allowed band projected onto the m axis, including some background. Figure 2(b) contains a Monte Carlo generated background distribution in m, properly normalized; its shape checks well with the real background events contained in the region outside the allowed bands in Fig. 1. Figure 2(c) then displays the subtracted event distribution. The subtraction below the peak amounted to 5% for the lowest energy setting and about 30% for the worst case, where the η cross section is small compared with multipion production. Data were taken at production angles $50° \pm 10°$ for photon energies from 0.925 to 1.45 GeV, at $70° \pm 10°$ from 0.81 to 0.93 GeV, and at $90° \pm 10°$ from 0.92 to 1.10 GeV. The data points from overlapping kinematical

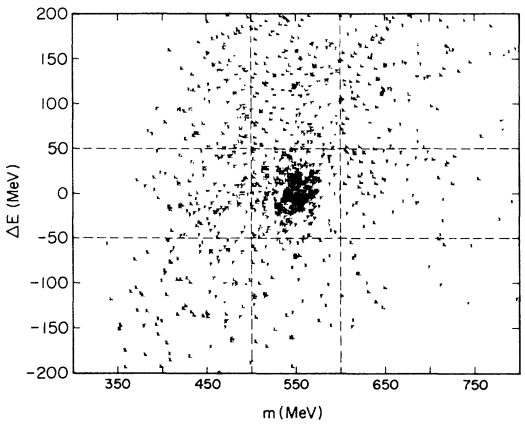

FIG. 1. ΔE plotted against m for a sample of 1000 events. Clustering of events at $\Delta E = 0$ and $m = 550$ MeV is due to eta production. The remainder are "background" events which do not satisfy η kinematics. The cuts placed at $m = 550 + 50$ MeV and $\Delta E = 0 \pm 50$ MeV were chosen to include all η events.

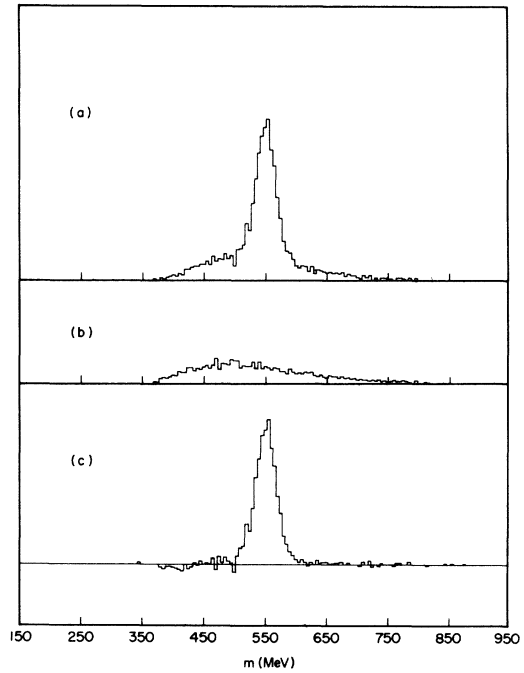

FIG. 2. Typical mass histograms showing (a) events from Fig. 1 for which ΔE falls within the allowed band, (b) Monte Carlo calculation of background events for same region as in (a), normalized to give the same amounts as seen in (a) outside the peak, and (c) results after subtracting (b) from (a).

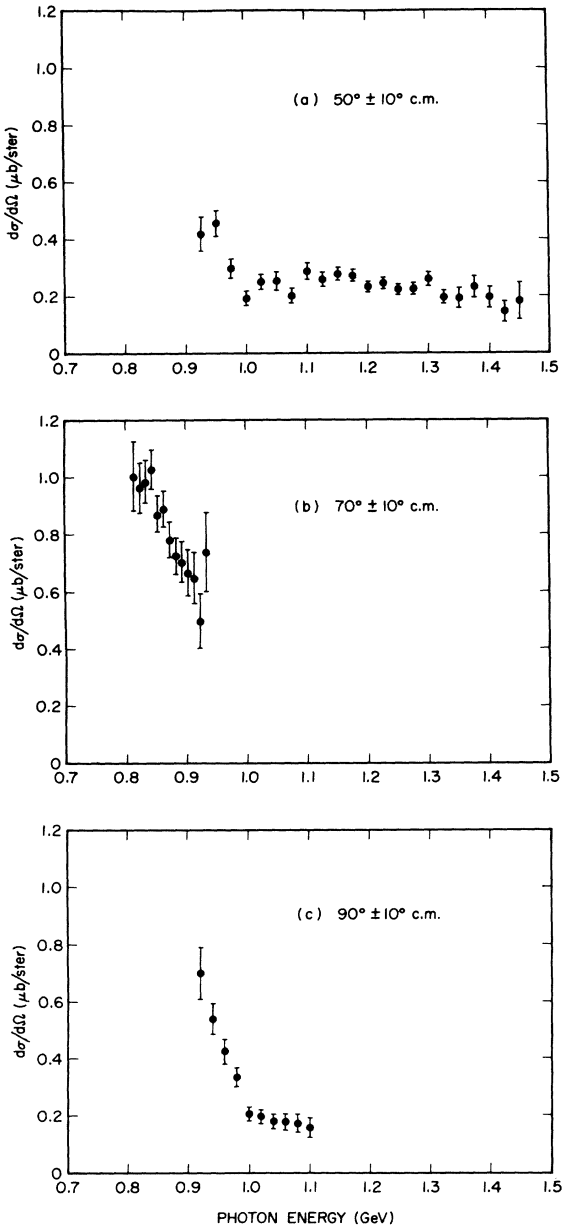

FIG. 3. Differential cross sections for three eta center-of-mass angles.

regions are consistent. The cross sections are displayed in Fig. 3.

The following features are clearly discernible: (1) There is a smooth, rapid decrease of the production cross section around 70°, on the high-energy end of the threshold enhancement. Its slope is less steep than indicated by earlier data[1,2] at 90°, and it occurs at lower center-of-mass energies than in $\pi p \to \eta n$.[10] (2) Within our errors, there is not much angular variation between 50 and 90° at energies between 0.9 and 1.0 GeV. However, above 1.0 and up to 1.1 GeV, there is a persistent tendency for the 90° cross section to lie 10-25% below the 50° values. (3) The 50° cross section remains roughly constant from 1.0 to 1.45 GeV; there is a small, but statistically significant dip between 1.0 and 1.1 GeV, which was also indicated in a previous experiment[4] and in $\pi p \to \eta n$[10] at the same c.m. energy, and a gradual, but small, decrease above 1.2 GeV.

These features permit the following remarks: (1) The more gradual slope of the 70° cross section as it decreases from its maximum value at about 0.84 GeV will be easier to fit with the nucleon pole and a resonant S_{11} wave[5] than the older data[1,2] seemed to allow. This still does not fully tie down the diagrams contributing to the large cross section between threshold and 0.9 GeV. Fuller angular distributions and polarization measurements will be necessary to probe for possible admixtures of other diagrams.

(2) The small difference between the 50° and the 90° cross section at $k \approx 1.02$ GeV confirms that the F_{15} (1688) isobar does not show up appreciably in η production [for pure F wave, the ratio would be $\sigma(50°)/\sigma(90°) \approx 2.5$].

(3) No direct-channel pole is likely to have a dramatic influence on process (1) above the threshold enhancement. While our measurements above 1.1 GeV cover a 20° angular region only, the essentially flat cross section behavior observed is not expected to conceal some violent behavior with energy at other angles.[11] To help further towards an unambiguous understanding of the η-nucleon system in this energy region, an experiment is presently under way to determine the recoil nucleon polarization in the critical region between 0.85 and 1.1 GeV.

---

*Work supported in part by the U. S. Atomic Energy Commission. Prepared under Contract No. AT(11-1)-68 for the San Francisco Operations Office, U. S. Atomic Energy Commission.

†Now at Stanford Linear Accelerator Center, Stanford, California.

[1]See, e.g., the compilation in the review talk of J. D. Jackson, in Proceedings of the Thirteenth International Conference on High Energy Physics, Berkeley, 1966 (University of California Press, Berkeley, Calif., 1967).

[2]C. Bacci, G. Penso, G. Salvini, C. Mencuccini, and V. Silvestrini, Nuovo Cimento 45A, 983 (1966).

[3]C. Bacci, R. Baldini-Celio, C. Mencuccini, A. Reale, M. Spinetti, and A. Zallo, Phys. Rev. Letters 20, 571 (1968).

[4]C. A. Heusch, C. Y. Prescott, E. D. Bloom, and

L. S. Rochester, Phys. Rev. Letters 17, 573 (1966).
[5]S. R. Deans and W. G. Holladay, Phys. Rev. 161, 1466 (1967), and references therein.
[6]C. Lovelace, in Proceedings of the International Conference on Elementary Particles, Heidelburg, Germany, 1967, edited by H. Filthuth (North-Holland Publishing Company, Amsterdam, The Netherlands, 1968); P. Bareyre, C. Bricman, and G. Villet, Phys. Rev. 165, 1730 (1968).
[7]C. A. Heusch, C. Y. Prescott, and R. F. Dashen, Phys. Rev. Letters 17, 1019 (1966).
[8]C. A. Heusch and C. Y. Prescott, Nucl. Instr. Methods 29, 205 (1964).
[9]For details of experimental method and data analysis, see L. S. Rochester, thesis, California Institute of Technology, 1968 (unpublished).
[10]W. B. Richards et al., Phys. Rev. Letters 16, 1221 (1966); and W. B. Richards, University of California Radiation Laboratory Report No. UCRL-16195, 1965 (unpublished).
[11]Lovelace's list of resonances (Ref. 6) found in πN phase-shift analyses mentions, for the $I=\frac{1}{2}$ channel, only one candidate in good standing which might show up in our energy region, in addition to the F_{15} and D_{15} states around 1680 MeV. This is the S_{11} (1709), with an elasticity of Γ_{el}/Γ_{tot} of 0.786 in $\pi N \to \pi N$. Whether this state, with a total width of $\Gamma \approx 300$ MeV, can account for the apparent shoulder observed in this experiment around 1.1 GeV remains to be established. A general tendency for forward peaking of the cross section is expected with increasing energy because of diagrams in the t channel (vector-meson exchange).

MEASUREMENT OF THE BRANCHING RATIO $(K_L \to \gamma\gamma)/(K_L \to 3\pi^0)$†*

M. Banner,‡ J. W. Cronin, J. K. Liu, and J. E. Pilcher
Palmer Physical Laboratory, Princeton University, Princeton, New Jersey
(Received 16 August 1968)

We have measured the branching ratio $(K_L \to \gamma\gamma)/(K_L \to 3\pi^0)$ to be $(2.24 \pm 0.28) \times 10^{-3}$. Combined with a recently reported branching ratio $(K_L \to 3\pi^0)/(K_L \to \text{all modes}) = 0.209 \pm 0.011$, we find $(K_L \to \gamma\gamma)/(K_L \to \text{all modes})$ to be $(4.68 \pm 0.64) \times 10^{-4}$.

An experiment to measure $K_L \to \pi^0\pi^0$ and $K_L \to \gamma\gamma$, previously reported in preliminary form,[1] has been repeated with an improved apparatus. We report here the results obtained for the decay rate of $K_L \to \gamma\gamma$.

The apparatus consisted of a pair spectrometer placed parallel to a K_L beam at the Princeton-Pennsylvania Accelerator. The spectrometer has been described in Ref. 1. In principle, a measurement of the energy spectrum of single γ rays in the c.m. system allows one to distinguish between the decay modes $K_L \to \gamma\gamma$, $K_L \to \pi^0\pi^0$, and $K_L \to 3\pi^0$. However, no kinematic check that the γ rays came from K_L is possible. To provide such a check, steel-plate spark chambers have been added to convert the additional γ rays.

Figure 1(b) shows a view of the apparatus looking upstream along the beam line. We have surrounded the remaining three sides of the beam with spark chambers. Each chamber consists of three 0.86-g/cm² aluminum plates nearest the beam, followed by 20 2.5-g/cm² stainless steel plates. The total thickness of each chamber, as measured along its normal, is 3.6 radiation lengths. The spark chambers extend along the beam for 10 feet, as is shown in the plan view of Fig. 1(a), and were viewed in small-angle stereo. The precision of spark location was 0.1 in. perpendicular to the beam, and 0.5 in. parallel to the beam.

These spark chambers were triggered along

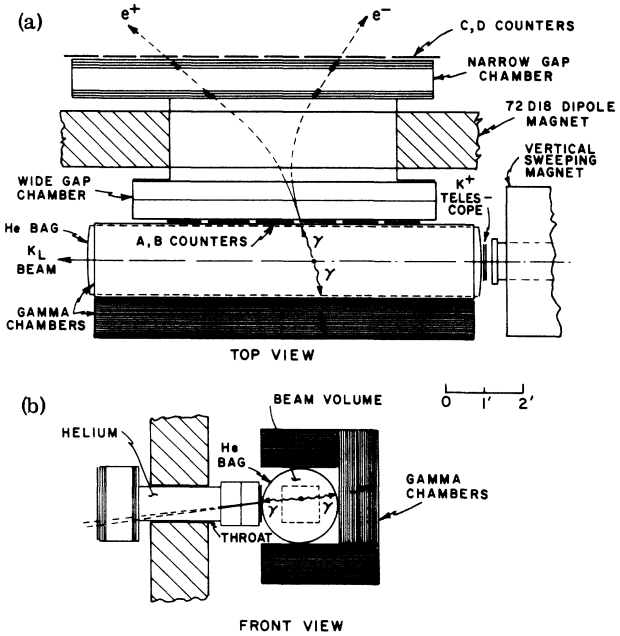

FIG. 1. (a) Plan view of apparatus. (b) End view of apparatus.